J Mater Sci (2006) 41:5941–5953
DOI 10.1007/s10853-006-0329-8

# Micromechanical analysis of an elastomer filled with particles organized in chain-like structure

**E. Coquelle · G. Bossis · D. Szabo · F. Giulieri**

Received: 7 April 2004 / Accepted: 7 July 2005 / Published online: 8 July 2006


**Abstract** Organization of iron filler particles inside an elastomer is obtained by curing the polymer in presence of a magnetic field. We have studied the effect of structuring the particles in chains on the quasistatic behavior in elongation in the absence of magnetic field. The effect of a coupling molecule between the surface of the particles and the elastomer is also analyzed. It is shown that the modulus of the first loading curve is strongly increased by structuring the particles, and also by the use of a coupling agent. Using an effective medium approach we well reproduce the experimental behavior of the elastic modulus and we deduce that a thick layer of elastomer is still present between the particles. A finite element calculation allows to distinguish between two modes of rupture at high strains, depending on the strength of the coupling between the particles and the matrix.

## Introduction

Electro and magnetorheology is a topic of growing interest since the eighties, in particular for applications dealing with damping. For instance, the automotive industry is interested in developing applications like engine mounts, shock absorbers, seat damping [1]. A more ambitious project concerns damping for seismic protection [2] using a MR fluid. All these applications are possible thanks to the ability to rapidly and reversibly change the rheological properties by applying an electric or a magnetic field. One can distinguish two classes of materials: one where the particles are embedded in a liquid (e.g. ferrofluids, magnetorheological fluids [3, 4]) and another one where they are embedded in solids (foams, elastomers), and two kinds of control: electric or magnetic. The main disadvantage of the first class is related to the sedimentation or segregation of particles in the presence of gravity or hydrodynamic forces. The second class of materials and more especially magnetorheological elastomers where magnetic particles are dispersed in a polymer do not suffer from this problem. On the other hand their adaptive character, that is to say the ability to change their elastic properties with the help of a magnetic field depends on the initial structure of particles inside the elastomer matrix. If the particles are dispersed homogeneously inside the elastomer, then the application of a field has practically no influence on the elastic properties. On the contrary if the particles have been aligned into columns before curing, then a large change of elastic properties can be observed in the presence of a magnetic field [5–7]. The most efficient magnetorheological effect is reported for low strains (around 5% of deformation) [8], but some authors found a field induced change till a strain of 40%. Actually a good understanding of the magnetorheology of such an elastomer is very dependent on the knowledge of microstructure (arrangement of particles inside the elastomer) and also on the interface between particles and elastomer.

In this paper we study the elastic behavior of the composite with the help of a micromechanical analysis based on a cell model in order to predict the elastic behavior of the composite in the absence of a magnetic field. We shall

E. Coquelle · G. Bossis (✉) · D. Szabo
LPMC, UMR6622, Université de Nice Sophia-Antipolis, Parc Valrose, 06108 Nice-Cedex 2, France
e-mail: georges.bossis@unice.fr

F. Giulieri
CMOM, Université de Nice Sophia-Antipolis, Parc Valrose, 06108 Nice-Cedex 2, France

use linear elasticity for the analytical model and the predictions will be compared with Finite Elements Methods (FEM) using non-linear elasticity and with experimental results. In section Sample preparation, we describe the sample preparation, and in section Quasi-static experiments the experimental results concerning the elasticity, with or without chemical modification of the surface of the particles. In section Theory a theoretical analysis is presented, and the comparison with experiments is shown in section Comparison between theory, FEM and experiments. We end up with a discussion and a conclusion.

## Sample preparation

The elaboration of a structured composite requires special care. First of all, concerning the choice of the elastomer, one needs good mechanical properties, but also a relative low viscosity before crosslinking, to facilitate the particles dispersion and its structuring. Moreover, a reticulation at room temperature (RTV) is a great advantage, in order to apply a magnetic field on the sample without need of specific or complicated devices. For all those reasons, our choice came to the Rhodorsil RTV 1062S (initial viscosity = 45 Pa s). The particles used to fill the elastomer needs good magnetic properties: no remnant magnetization and high saturation magnetization. We used a RP Normapur iron powder, with a high degree of purity (99.5% of iron). Moreover, the particles are near to be perfect spheres, because this iron powder has been prepared by hydrogen reduction. SEM experiments have proven a good spherical shape and a not too large size dispersion (between 2 and 10 μm) of the powder (Fig. 1).

The first step is a chemical clean-up of the particle, to remove their impurities and to get a reproducible surface. Using an ultrasound sonicator, one washes them successively with trichloroethylene, ethanol, pure water, ethanol and acetone, 10 min each. The last and most important step consists in coating the particles with a silane coupling agent to improve adhesion to the elastomer: a 5% solution of aminosilane is prepared in pure water; the iron powder is then blended inside the solution still using the sonicator. The treated powder is at last washed using ethanol and then dried under vacuum. Actually in this study we shall use both coated and not coated particles.

Then, particles are carefully dispersed in the elastomer. However, loading the pre-polymer strongly increases its viscosity, so only 10% in volume of iron particles is included in the matrix; higher loadings are possible, but some silicone oil has to be added to the melt to reduce its viscosity and keep molding and particle structuring easy. The melt is degassed under vacuum, molded in a cylinder which is placed inside an electromagnet and put on rotation in order to avoid sedimentation and help the particles to find their minimum of energy in presence of the field. The following two steps structuring protocol has been established. The first step is devoted to the structure creation, and lasts 10 min. For this time, the melt still has a low viscosity; the field is slowly raised up to 200 kA/m at a mean rate of 20 kA/m per minute (to prevent a too fast and out of equilibrium aggregation). Then, as the viscosity increases, we start the second step: the field is kept at its higher value for 10 min till curing is almost completed, then we drop it to half of its value for 4 h, and finally decrease it to 0. The sample can be unmoulded after one day, and is ready to use after one week. Figure 2 illustrates the anisotropic structure one can get: near-to-be perfect chains well oriented in the direction of the magnetic field.

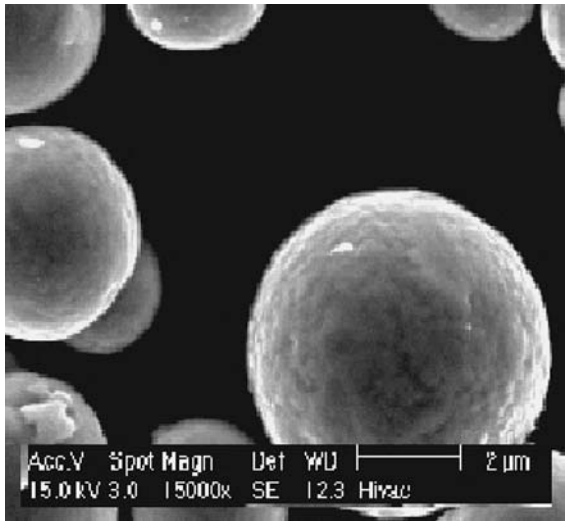


**Fig. 1** Carbonyl iron particles viewed by SEM

## Quasi-static experiments

The quasi-static behavior of the composite under traction is investigated thanks to a home made traction device. The samples are cylinders whose length is 50 mm, and diameter 7 mm.

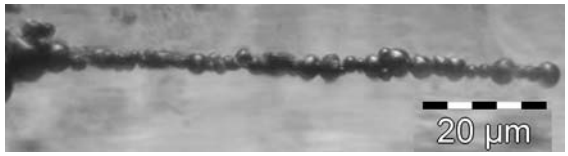


**Fig. 2** A chain of the structured composite viewed by optical microscopy at low volume fraction (Φ = 3%) inside a transparent elastomer

Pure elastomer

In order to understand the behavior of the composite, we need to determine the stress–strain curve for the pure elastomer. Figure 3 shows the experimental result of the uniaxial tension of a cylindrical sample. We see that the linear Hookean model is only valid till $\lambda = 1.4$, but could be roughly valid up to $\lambda = 3$.

It is well known that at high strains the stress–strain law should be a non-linear, hyper elastic one. In the literature related to rubber elasticity, one can find many theoretical models; most of the approaches are based on a strain energy density function or elastic potential $W$, corresponding to the change in the Helmoltz free energy of the material upon deformation. We have chosen the well-known Mooney–Rivlin law: its third-order deformation approximation perfectly fit our elastomer behavior, as it can be seen in Fig. 3. The strain energy function is [9]:

$$W_{\mathrm{MR-5p}} = c_{10}(I_1-3)+c_{01}(I_2-3)+c_{20}(I_1-3)^2 + c_{11}(I_1-3)(I_2-3)+c_{02}(I_2-3)^2+\frac{1}{d}(J-1)^2 \quad (1)$$

- The subscript MP-5p stands for Mooney–Rivlin, five parameters
- The constants $c_{ij}$ are chosen to fit a 1D tension of a pure elastomer cylinder, while keeping a physical meaning, to ensure convergence for our FEM calculations.
- $d = 2/K$ where $K$ is the bulk modulus of the elastomer
- $J$ is the ratio of the deformed elastic volume over the undeformed volume of materials.
- $I_1$, $I_2$ and $I_3$ are the strain invariants, given by

$$I_1 = \lambda_1^2+\lambda_2^2+\lambda_3^2$$
$$I_2 = \lambda_1^2\lambda_2^2+\lambda_2^2\lambda_3^2+\lambda_3^2\lambda_1^2$$
$$I_3 = \lambda_1^2\lambda_2^2\lambda_3^2 \quad (2)$$

The $\lambda_i$ are the principal stretch in the $i$ direction, and are defined by the ratio of the final length to the initial one. The quantities $(I_1 - 3)$, $(I_2 - 3)$ and $(I_3 - 3)$ conventionally impose $W$ to be zero in the non-stained state.

The third invariant $I_3$ represents physically the square of the ratio between the volume of a material element in the deformed and undeformed state. As elastomers are nearly incompressible, $I_3 = 1$.

The geometry of the sample is a cylinder so the deformations in the transverse directions are the same. Hence,

$$\lambda_2 = \lambda_3 = \frac{1}{\sqrt{\lambda}} \quad (3)$$
$$I_2 = I_3$$

So, the stress–strain law is:

$$\sigma_{\mathrm{MR}} = 2\left(\lambda-\frac{1}{\lambda^2}\right)\left(C_{10}+\frac{C_{01}}{\lambda}+2C_{20}\left(\lambda^2+\frac{2}{\lambda}-3\right) +2\frac{C_{02}}{\lambda}\left(2\lambda+\frac{1}{\lambda^2}-3\right)+3C_{11}\left(\frac{1}{\lambda^2}-\frac{1}{\lambda}+\lambda-1\right)\right) \quad (4)$$

Writing $\lambda = 1 + \epsilon$, the coefficient of the first power in $\epsilon$, gives the initial Young modulus: $6(C_{10} + C_{01}) = E_{\mathrm{initial}}$

The fit of the experimental curve for a 1D tension of an elastomer cylinder (Fig. 3) with a 5 parameters

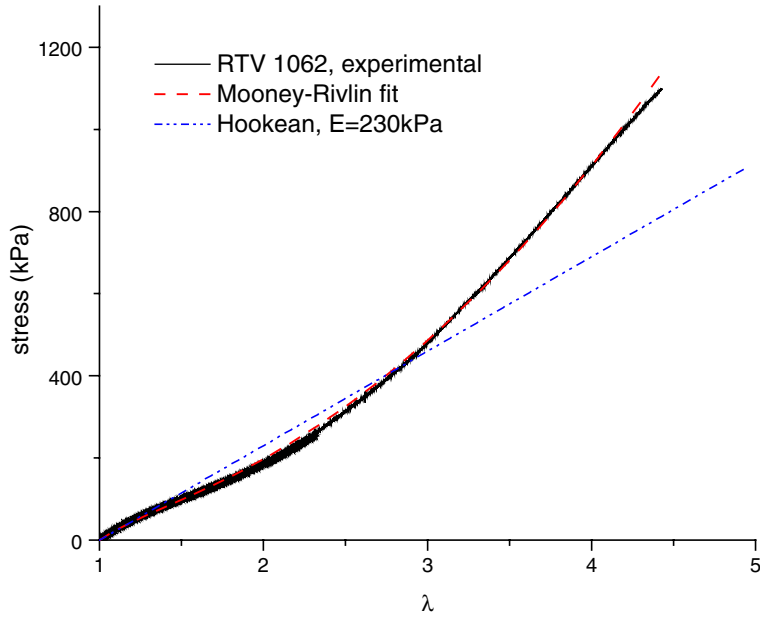


**Fig. 3** Uniaxial tension stress–strain curve of the RTV 1062 S elastomer

Mooney–Rivlin law well represents the experiment with the following coefficients:

$$C_{10} = 13680\text{Pa}, C_{01} = 39000\text{Pa},$$
$$C_{20} = C_{02} = 0\text{Pa}, C_{11} = 9720\text{Pa}$$

The corresponding initial Young modulus of the pure elastomer is then: $E_m = 316$ kPa. Note that this initial modulus is well above the one of 230 kPa that can approximate the experimental behavior till a stretch value $\lambda = 3$. For the analytical model where we need to use linear elasticity to represent the pure elastomer behavior on the wider possible range, we shall use the average value $E = 230$ kPa, but for finite element calculations we use Eq. 4 with the values of $C$ listed above.

## The composite

For the traction experiments with the filled composite, one must take care of the decrease of stiffness between the first and subsequent tractions [10, 11]. This effect is clearly seen in Figs. 4 and 5. Most of the softening effect-known as Mullins effect—occurs during the first load and, after a few cycles, the composite gains a constant stress–strain behavior. Thus, during this first traction, the composite is damaged at some extent due to: particles' reorganization, aggregate breaking, debonding of the elastomer from the particles [12].

The relation between the Mullins effect and the debonding will be the subject of an other paper. Here we mainly wish to model the first traction curve of a structured composite; nevertheless, it is interesting to have a look to the difference between first and second traction curves in order to emphasize the effect of the organization in chains and/or of the coating molecule on the elasticity. In Fig. 4 we see that there is a very large difference of effective modulus (almost a factor of 2) between the sample structured and coated and the isotropic sample. The fact that in the isotropic sample there is no difference between the first and second traction means that the particles are far enough from each other-the volume fraction is 10%—so that the reinforcing effect does not depend on interaction between particles or on debonding. On the contrary for the structured sample the chains of particles behave as solid fibers that increase the modulus of the composite, but, as the strain increases, the local stress between two particles becomes much larger than the average stress, and the elastomer will progressively debonds. That is why the second traction curve is close to the one of the isotropic composite. Furthermore, we also expect a large difference between the cases where the particles are coated with a silane coupling agent or not, since breakage between the bonds should happen at higher strains when the adhesion between the elastomer network and the particles is stronger. That is what we observe in Fig. 5 where the difference between the first and second traction curves for the structured but uncoated sample is much smaller than for the coated one. These results demonstrate that the Mullins effect is here mainly due to debonding between the particles and the matrix. As our goal is to model the material behavior without any kind of damage, we shall focus on this first elongation for comparison with simulations and models. Thereafter, all the experiments presented are first traction curves realized with 10% iron fillers coated with a silane coupling agent, to strongly reinforce the charge-matrix adhesion.

In Figs. 6 and 7, we have plotted the first tension curves till high strains of the four classes of materials: structured

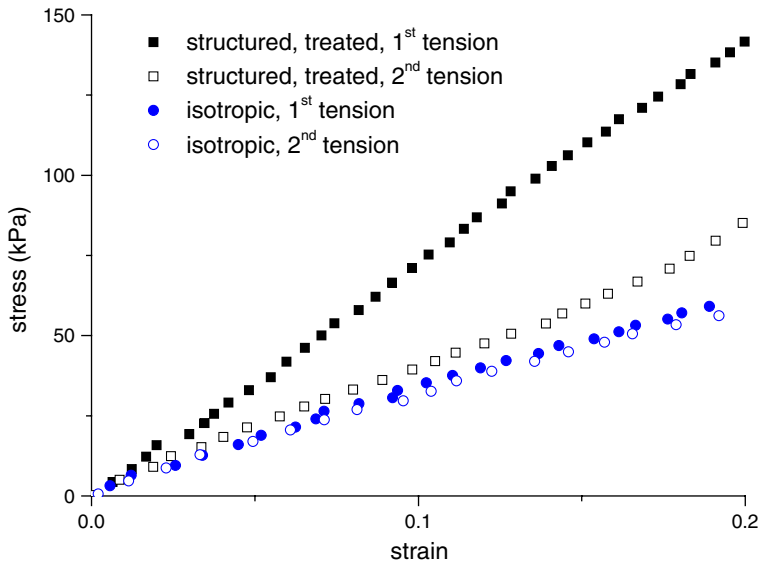


**Fig. 4** Difference between first and second traction curves of the structured, treated composite with respect to the isotropic composite ($\Phi = 10\%$)

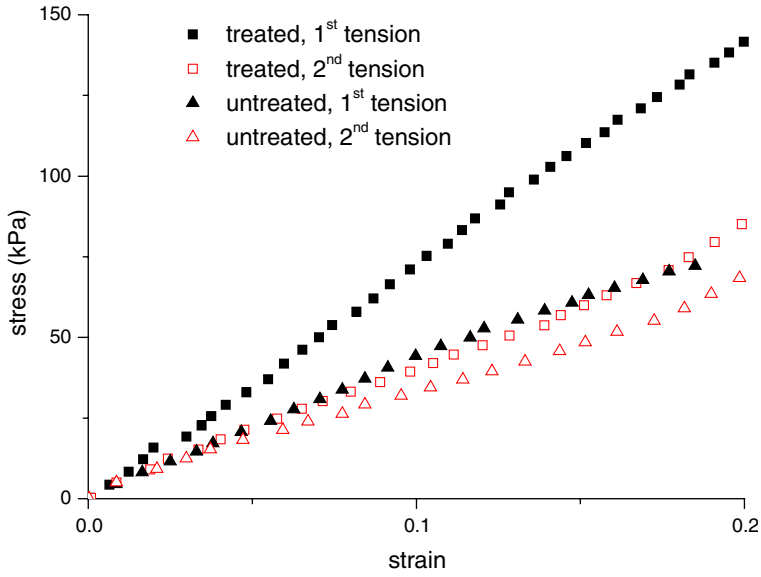


**Fig. 5** Difference between first and second traction curves for treated and non-treated particles (both in a structured composite, $\Phi = 10\%$)

composite with treated particles, structured composites with untreated particles, isotropic composite with treated particles and pure elastomer. As already told we see that, except at very low strains (below 0.05:cf. Fig. 7), the behavior of the untreated and structured composite becomes very similar to the one of the isotropic composite.

Also, as expected, the experiments reported in Figs. 6 and 7 show that the elastic modulus of a filled, non-structured composite is well above the pure elastomer one. The values of an effective modulus based on a strain of 2 ($\lambda = 3$) are reported in Table 1. The increase from the pure elastomer ($E = 230$ kPa) to the structured and coated composite ($E = 750$ kPa) is very large. because the pseudo-chains oriented in the direction of the load strongly increase strongly its stiffness; we shall see in section The structured composite, how this enhancement is related to the average size of the gap between the particles.

## Theory

### The isotropic material

We have compared in Fig. 8 the stress–strain experimental behavior of a filled, non-structured elastomer ($\phi = 10\%$) to the predictions of an effective medium theory and to the result of a FEM simulation whose model is described in section The structured composite. In effective medium

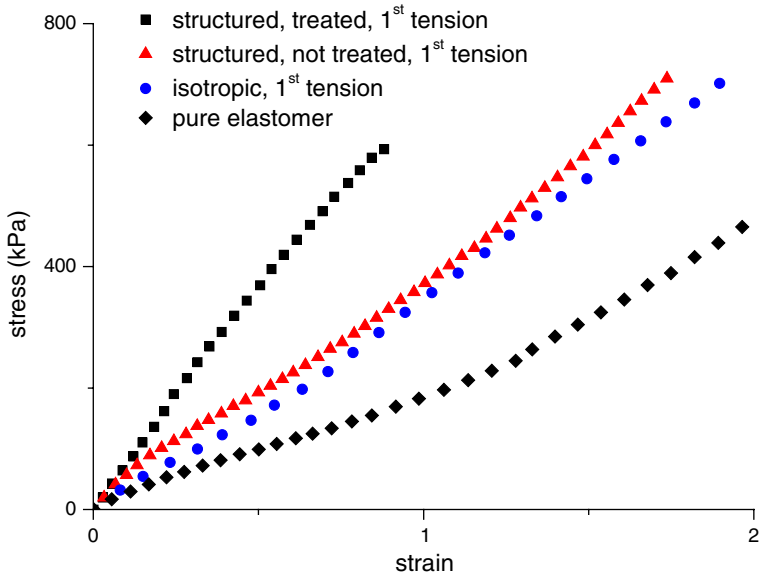


**Fig. 6** First uniaxial tensions of the studied materials till high strains

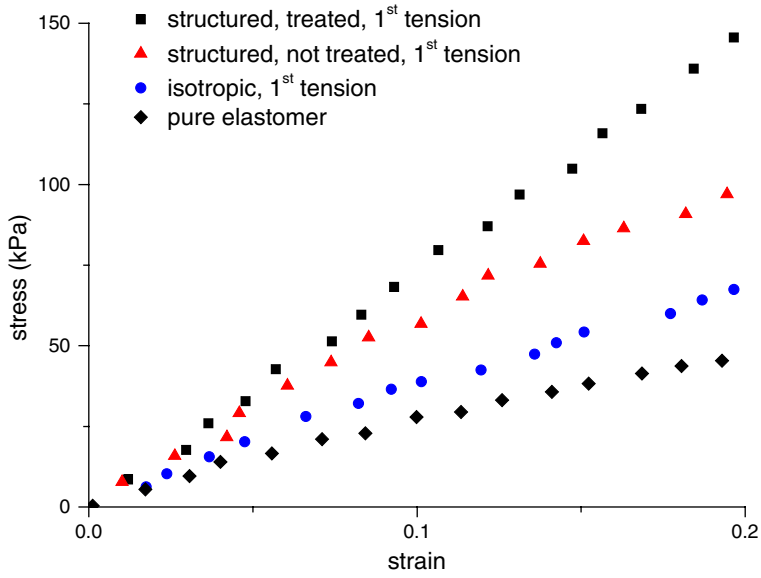


**Fig. 7** First uniaxial tensions of the studied materials (detailed view at low strains)

**Table 1** Average Young modulus of the studied materials for strains lower than 2

| Material | Average Young modulus (kPa) |
|---|---|
| Structured composite, treated | 750 |
| Structured composite, not treated | 420 |
| Isotropic composite | 370 |
| Pure elastomer | 230 |

theory the material is supposed to be linear and isotropic; and the effective Young modulus is calculated, based on the volume fraction Φ and the particles and matrix modulus. As the volume fraction is low, the effective modulus can be represented by [13]

$$G^* = G_m\left(1 - \frac{15\phi(1-\upsilon_m)(1-G_i/G_m)}{7-5\upsilon_m+2(4-5\upsilon_m)(G_i/G_m)}\right) \quad (5)$$

where $\nu_m$ is the Poisson ratio of the matrix, $G_m$ the shear modulus of the matrix is related to the Young modulus, $E_m$ by

$$G_m = \frac{1}{2}\frac{E_m}{1+\upsilon_m} \quad (6)$$

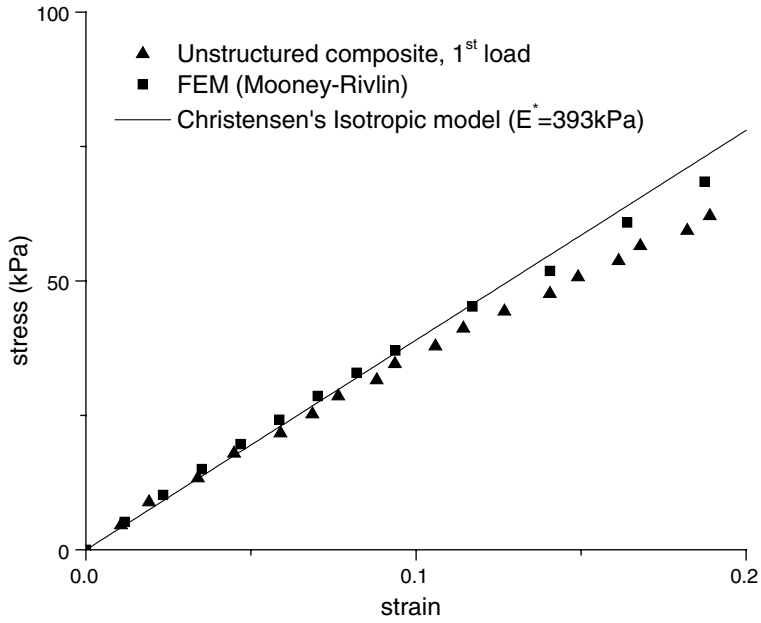


**Fig. 8** Experimental unstructured (isotropic) composite Φ = 10% compared with Christensen's isotropic model and FEM calculations

The same relation holds for $G_i$ the shear modulus of the particle. Considering the elastomer as linear (with initial modulus $E_m$ = 316 kPa given by the fit with Eq. 4), nearly incompressible ($\nu_m$ = 0.493), filled with pure-iron particles ($E_i$ = 196 GPa, $\nu_i$ = 0.29), we get an effective Young modulus of $E^*$ = 395 kPa, which is close to the experimental one ($E$ = 370 kPa) Actually, as the inclusion modulus is far higher than the matrix one ( $G_i \gg G_m$), Eqs. 5 and 6 reduce to the well known Einstein formula:

$$E^* = E_m(1 + 2.5\Phi) \tag{7}$$

## The structured composite

### *Analytical model*

In order to develop an analytical model that describes the behavior of a structured elastomer, we start from a micromechanical analysis, using a unit cell which can generate a representative chain by replication along the chain axis [14, 15]. This cell is a cylinder, an elementary part of the composite, and is made of two half-spheres embedded in a large cylinder of elastomer (Fig. 9). Applying boundary conditions described hereafter on the surface of this cylinder builds a chain structure in the displacement direction and an average medium in the transverse one.

The structure is regarded as made of equally spaced ideal particles, so the main parameter in the model is the ratio $g/a$ of the gap between the spheres to the radius. The quantity $L$ represents the thickness of an elastomer annulus, surrounding the particles. It is calculated as a function of $g/a$ ratio and volume fraction of inclusions $\phi$:

$$L + a = \sqrt{\frac{4a^2}{3\phi\left(2 + \frac{g}{a}\right)}}$$

As the cell is tested in uniaxial tension, the displacement is constant everywhere on the two terminal-sections of the cylinder. It is set to zero on the bottom section, while it is equal to $\epsilon(2a + g)$ on the upper one, $\varepsilon = \Delta l/l$ being the imposed strain. The lateral section is kept straight due to the presence of adjacent chains, but the average radius of the cylinder is allowed to decrease according to the Poisson ratio of the elastomer: $\Delta V = -\varepsilon V$.

We shall suppose that the linear elasticity can be used: Fig. 3 has shown it gives reasonable approximation till $\lambda$ = 3.

In the frame of linear elasticity, the effective modulus of the elementary cell can be calculated following Christensen [16]. He solved the mechanical equilibrium using the lubrication approximation, requiring the gap between the spheres being much smaller than the inclusion radius.

At the surface of the sphere, $z = \pm h/2$, the displacement field should satisfy:

$$\begin{aligned} u_r &= 0 \\ u_z &= \pm\frac{u}{2} \end{aligned} \tag{8}$$

In this case the displacement field is approximated by

$$\begin{aligned} u_r &= \frac{3}{4}\frac{u}{h} r\left(\frac{4z}{h} - 1\right) \\ u_z &= -\frac{3}{2}\frac{u}{h}\left(\frac{4z^3}{3h} - z\right) \end{aligned} \tag{9}$$

where $u$ is the displacement imposed on the system.

A map of the orientation of this displacement field is shown in Fig. 9. In Fig. 10 we compare the amplitude of the normalized deformation field (Eq. 9) to the one obtained by FEM using non linear elasticity as indicated in next section. We have done the comparison for two different strains: a moderate one $\epsilon_g$ = 0.25 and a strong one $\epsilon_g$ = 1.2. In Fig. 10 the comparison is made along the revolution axis and in Fig. 11 along the radial axis in the symmetry plane. In both cases the agreement is very good

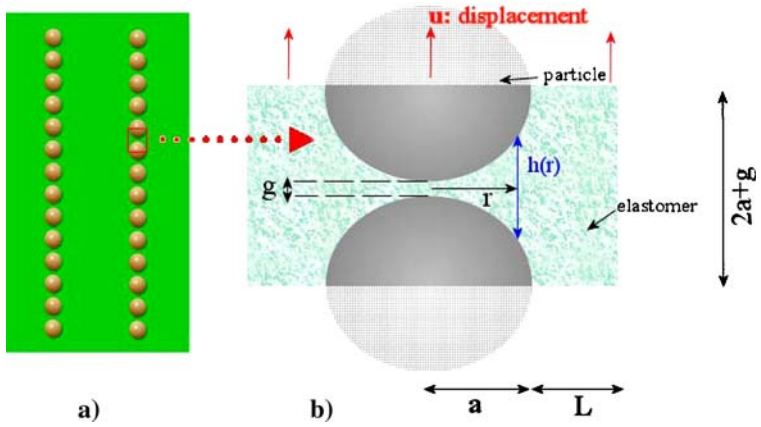


**Fig. 9** The chain model of the structured composite: (**a**) overview; (**b**) unit cell

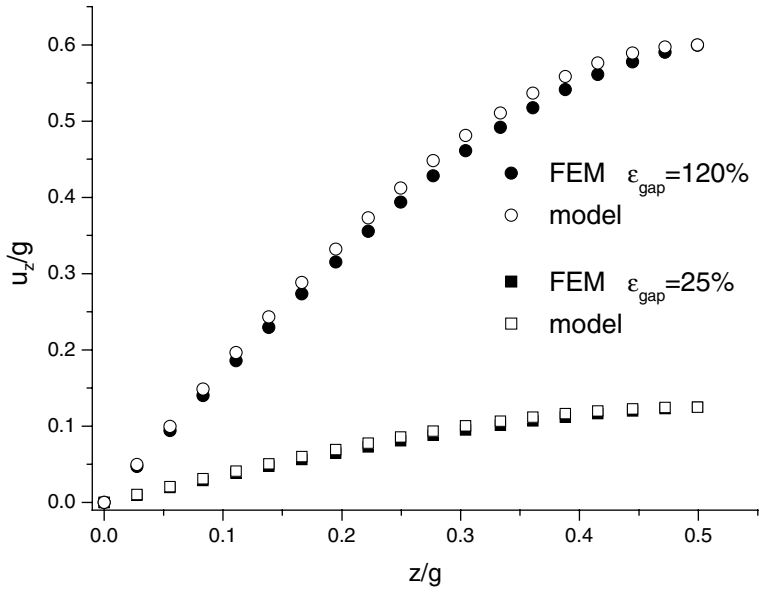


**Fig. 10** Normalized strain between two spheres along the revolution axis. Comparison between Eq. 9 and FEM model with Mooney–Rivlin law; initial gap:0.056 radius

along the revolution axis. Along the radial axis the agreement is fair at the lower strain but there is a quite large difference at higher strain, although the general shape is well reproduced. We shall have to keep in mind that at high strains the analytic model only reproduces approximately the displacement field in the gap, but nevertheless the overall stress–strain behavior is well reproduced even at high strain as we shall see in section Two spheres' experiment.

Expressing the change of gap length with the angle $\theta$; the strain energy between the two spheres is:

$$U = \frac{\pi}{8} E_m u a \int_0^{\pi/2} \frac{\sin^3\theta\cos\theta}{(g/2a + 1 - \cos\theta)^3} \mathrm{d}\theta \qquad (10)$$

whereas the deformation energy of an equivalent cylinder of radius a of elastomer is:

$$U = \frac{1}{2} E_{\mathrm{eff}} \left(\frac{u}{2a+g}\right)^2 \pi a^2 (2a+g) \qquad (11)$$

where: $E_m$ is the Young modulus of the elastomer (matrix), $E_{\mathrm{eff}}$ is the effective Young modulus, $u$ is the imposed displacement on the elementary cell, $a$ is the radius of the inclusions, $g$ is the gap between the spheres.

Identifying the strain energy of Eqs. (10) and (11) gives the effective modulus of the structured composite model:

$$E_{\mathrm{eff}} = \frac{1}{4} E_m \frac{(2a+g)}{a} \int_0^{\pi/2} \frac{\sin^3\theta\cos\theta}{(g/2a + 1 - \cos\theta)^3} \mathrm{d}\theta \qquad (12)$$

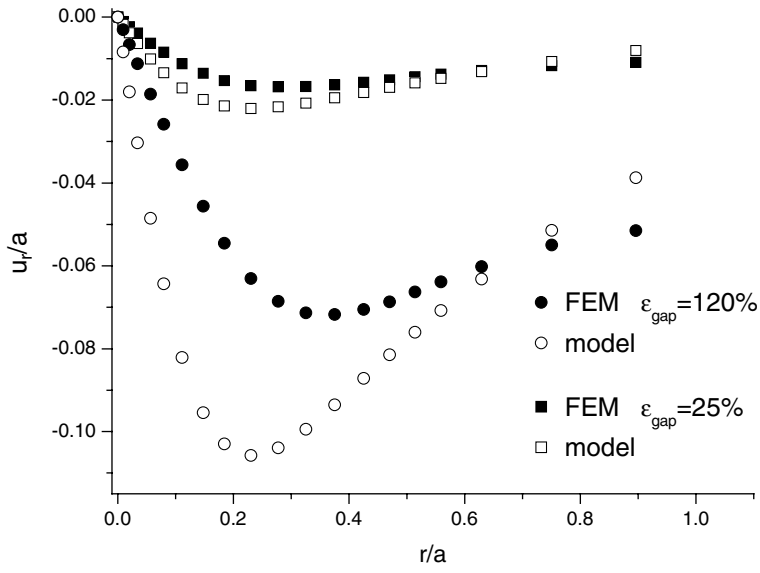


**Fig. 11** Normalized strain between two spheres along the radial axis. Comparison between Eq. 9 and FEM model with Mooney–Rivlin law, initial gap:0.056 radius

However, we still have to add an annulus of elastomer of thickness $L$ which is supposed homogeneously strained; so the total stress is given by

$$\sigma = \frac{E_{\text{effective}}\varepsilon a^2 + E_{\text{m}}\varepsilon\left[(a+L)^2 - a^2\right]}{(a+L)^2} \tag{13}$$

As this solution is obtained in the frame of linear elasticity, finite elements calculations were made in order to get a more accurate solution and to check the range of validity of these approximations.

*FEM backgrounds*

The goal of these simulations is first to check the validity range of the analytical model, and also to get a more precise view of stresses inside the gap between two particles.

The elements used in the simulation have four degrees of liberty ($X$, $Y$, $Z$ and the hydrostatic pressure), and are designed for the Mooney–Rivlin law.

The FEM system is stretched in the $Z$ direction. Moreover, as our elementary cell is the unit part of the chain-like structure, it is clear that the contact lines between neighbors cell must remain straight during extension to keep the continuity of the system; so a displacement is imposed on the vertical border with three constraints: keep the borders straight, preserve the volume of the elastomer (according to its Poisson ratio), and reach an equilibrium at the end of the simulation (the X component of the force on the lateral nodes is zero). No stresses are imposed on the lateral part of the cylinder. So, the edges would not deform, as inside the composite.

Perfect bonds between the elastomer and the inclusion were assumed. The solid sphere is taken to be perfectly rigid, so as to all the deformation energy is stored in the matrix.

## Comparison between theory, FEM and experiments

Two spheres' experiment

In order to have an experimental model of the unit cell we have made a sample where two macroscopic spheres (2 cm in diameter) are embedded in an elastomer as shown in Fig. 12. The size of the gap between the two spheres is set to 1 mm. To be able to access high strains without desadhesion at the surface of the spheres, their surfaces are chemically modified to improve the elastomer to surface adhesion. Basically, the method is the same as the one formerly presented but the spheres are placed in the silane solution without sonification.

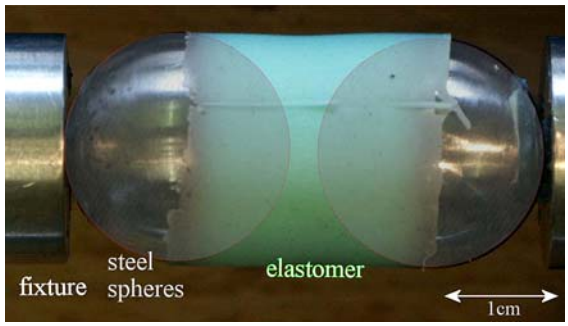


**Fig. 12** The two spheres experimental system. The spheres diameter is 9.8 mm, they are spaced by 1 mm and are embedded in elastomer

The comparison of the model to FEM and experiments shows a very good agreement till the rupture between the elastomer and the particles at a strain (relative to the gap) of 4 (cf. Fig. 13). The analytical model (Eq. 14) based on the average modulus of the pure elastomer (i.e. 230 kPa) will predict a straight line since the model is linear and so will not reproduce the small curvature of the experimental curve. Nevertheless the curve obtained without any parameter gives a quite fair estimation of the experimental behavior and so can be safely used for the purpose of modeling the effective modulus of the structured composite.

At the breaking point with a local strain of 4, the highest local stress found by FEM is located just at the middle of the two spheres and reaches 1.1 MPa.

Gap between particles in the structured composite

The only parameter of our model is the gap between particles. We have used the analytical approach at low strains ($\epsilon < 0.1$) in order to fit the value of the gap from the experimental curves, the best fit is obtained with $g/a = 0.056$ (cf. Fig. 14). Of course one must keep in mind that the real microstructure of a structured composite is far from the idealized one and that this gap represents an average one.

This value $g/a = 0.056$ is in quite good agreement with the one obtained from permeability measurements in the same kind of structured composite [13], which gives $g/a = 0.06$. The existence of a gap filled by elastomer between particles can be evidenced by electronic microscopy. Some in situ investigation has been made, by cutting longitudinally the samples using a cryotome. This device freezes the composite, and then a knife cut it in thin sheets of 15–20 μm depth. The sheets are observed by SEM. One can see the gap between the particles (cf. Fig. 15) and the order of magnitude is actually the one we have found from the fit of elastic properties. The existence of a gap between particles was rather unexpected since a high magnetic field is used to structure the particles. For a small gap between

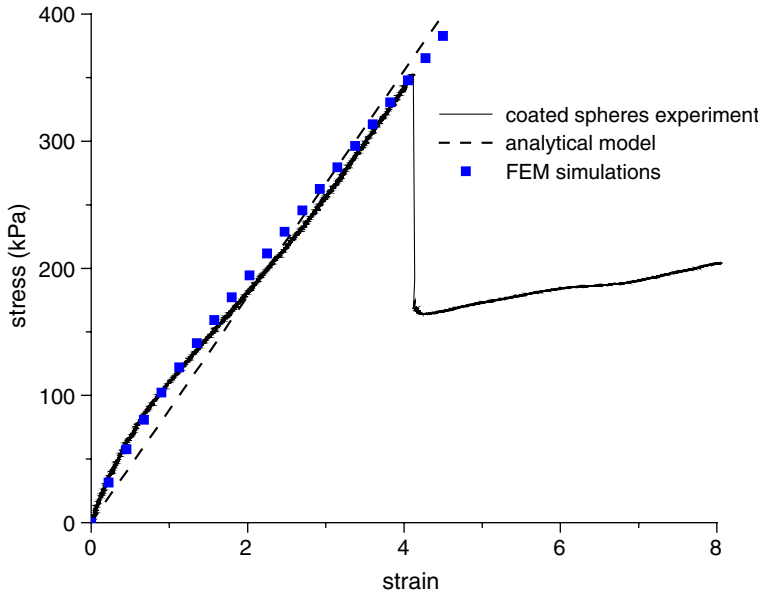


**Fig. 13** Comparison between experiments, FEM and model on the two grafted spheres system. The breaking inside the matrix occurs at $\epsilon_{gap} = 410\%$, at a mean stress of 350 kPa

the particles, the lubrication theory predicts a friction coefficient that is the Stokes' one divided by the normalized gap $g^* = g/a$ between the surfaces. Naming $F_{magn}$ the attractive magnetic force between the particles, the relative velocity is given by

$$\frac{dg^*}{dt} = \frac{F_{magn} g*}{6\pi\eta a^2} \tag{14}$$

This relation takes into account the slowing down due to lubrication, it is only valid for small separations ($g^* < 0.1$) but for the sake of evaluation we can use it at larger distances. Moreover, at high magnetic field ($\mu_0 H = 0.5$ Tesla), we consider that the magnetization has reached its saturation value $M_s$, so the magnetic force can be written is the dipolar approximation as:

$$F_{magn} = \frac{6m^2}{4\pi\mu_0 r^4}$$
$$m = \mu_0 M_S \frac{4}{3}\pi a^3 \tag{15}$$

The saturation magnetization $M_s$ is 1.713 $10^6$ A $m^{-1}$ for iron.

Starting form a separation of three diameters between surfaces (initial state for a volume fraction $\Phi = 10\%$) and ending with $0.06a$, the approach time is around 6 ms for a viscosity $\eta = 45$ Pa s. This is much shorter than the

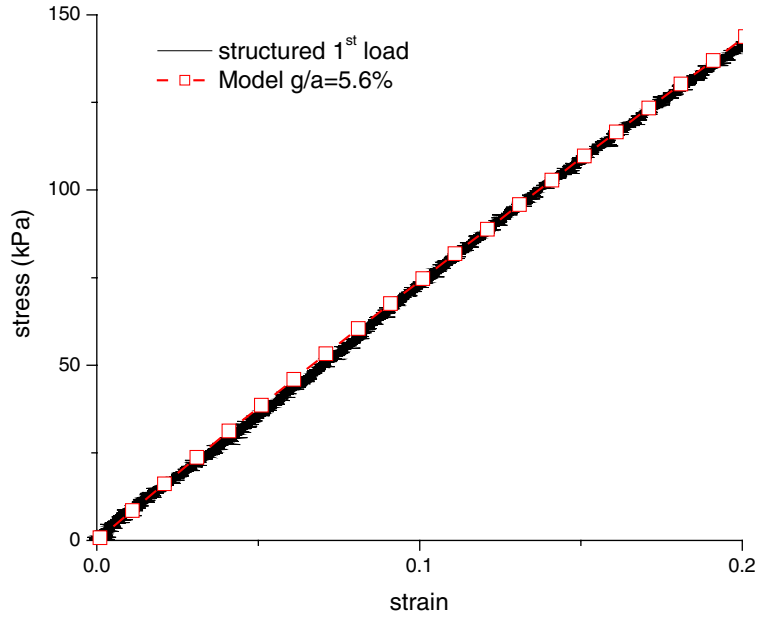


**Fig. 14** Comparison between the experimental uniaxial tension of the structured composite ($\Phi = 10\%$) and the model for a ratio $g/a = 5.6\%$

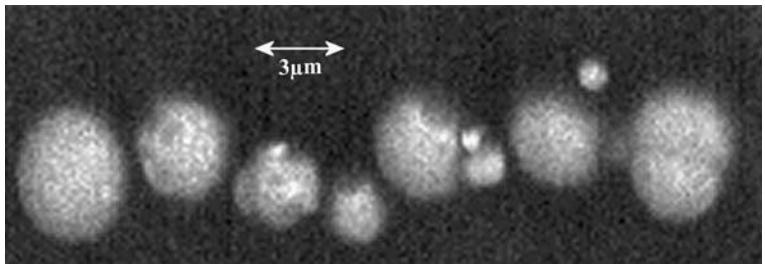


**Fig. 15** SEM view of a chain inside the structured composite, obtained by cutting a thin sheet of the material

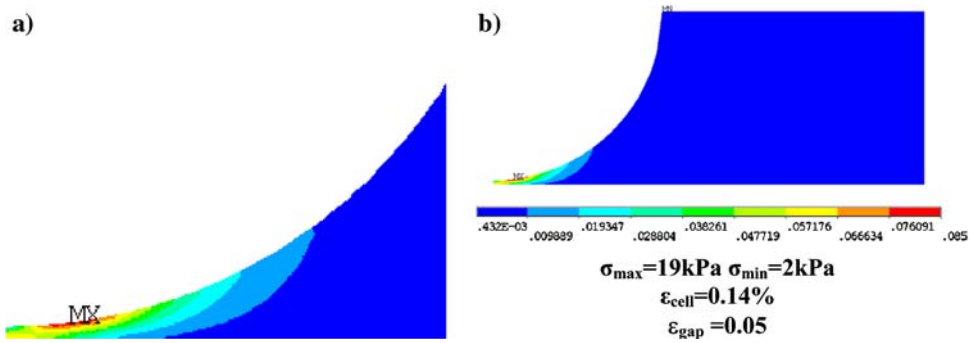


**Fig. 16** Strain field calculated by FEM on the unit cell (**a** and **b**) for $\epsilon_{gap} = 0.05$ The maximum local stress (19 kPa) is found at the surface of the particle (**a**)

experimental time during which a high field is applied before curing. One explanation could be related to the physical adsorption of a thick layer of polymer chains onto the particle, which offers a very high resistance to the approach of the two particles.

## Stresses inside the gap

Due to the small gap between particles, some regions between the poles can access very high stresses. We present an analysis by FEM of the strain map in the following Figs. (16, 17, 18), for three different strains and starting with a gap $g = 0.056a$.

On all the figures the first principal strain map is plotted; the darkest regions are less strained than the lighter ones.

First of all, the first principal strain map reveals the surrounding block of elastomer is weakly deformed, whatever the imposed strain is. On the other hand, the stress concentrates in the region between the spheres, and the direction of the local stress is clearly heading toward this region. This means that the main effect of the elastomer incompressibility is to concentrate all the stress towards the middle of the gap. For more convenience, strains are reported relatively to the gap.

Another interesting point is the location of the highest stress. For the smallest strains, till $\epsilon_{gap} = 0.3$, the highest stresses are located at about 15° from the pole, on the surface of the inclusion, whereas for larger deformations, the most stressed region migrates inside the elastomer, just to the middle of the gap. For instance, in Fig. 16, the maximum stress on the pole is 20 kPa, whereas just at the middle of the gap the local stress is 18 kPa. In practice, in the case of weak bonds between the elastomer and the inclusion, one can expect the damage will begin from the surface of the sphere, near its pole, with a minimal size of 30°. Now, if the particles are coated with a coupling agent, the bonds between the elastomer and the inclusion become much stronger, and consequently one can expect the elastomer starts tearing from the middle of the spheres once a

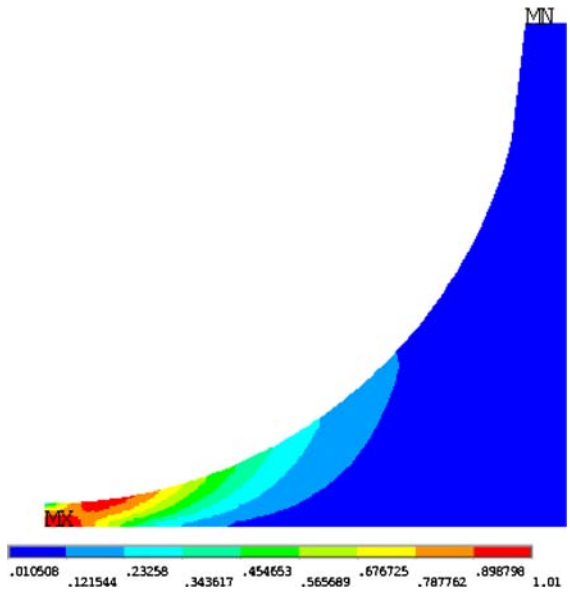


**Fig. 17** Strain field for $\epsilon_{gap} = 1.25$. $\sigma_{max} = 380$ kPa, $\sigma_{min} = 13$ kPa, $\epsilon_{cell} = 3.4\%$

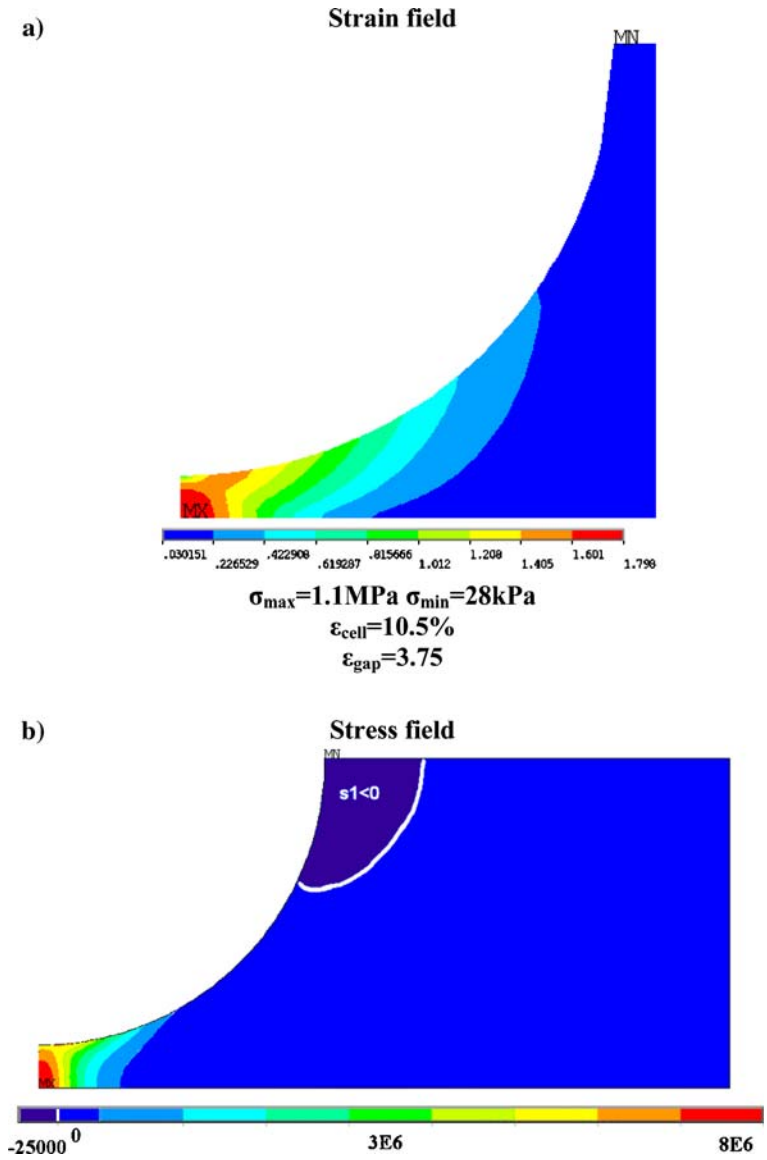


**Fig. 18** Strain (**a**) and stress (**b**) field for $\epsilon_{gap} = 3.75$

critical energy is reached. We can estimate the critical strain above which tearing of the elastomer will occur by taking the local tearing stress of 1.1 MPa obtained from a comparison of experiments and FEM on a two spheres system. In the unit cell representing the composite we reach this stress at the middle of the gap for an average strain of 10.5%. If we calculate the average breaking strain from the local breaking strain $\epsilon_g = 4.1$ in the two spheres experiment we obtain $\epsilon = \epsilon_g/(1 + 2/0.056) = 0.11$ which is close to the value obtained from FEM. Actually we do not see any inflexion on the stress–strain curve of the composite material at this point but rather a progressive departure from a straight line starting at about $\epsilon = 0.3$ (cf. Fig. 6); this is obviously because we have a distribution of gaps rather than a constant one.

In the upper part of Fig. 18 we have plotted the first principal strains at the breaking point while the lower part contains the first principal stress. This last quantity measures the hydrostatic intensity of the stress state. It is seen that both fields are very similar. In the stress field, the white line delimits the positive and negative stress domain; the zone of maximum hydrostatic extension is found in the gap, between the particles' poles (8 MPa), while the maximum hydrostatic compression (–25 kPa) surrounds the spheres.

Moreover, the strain map reveals the stress sharply changes only for angles smaller than 60°. For example, for $\epsilon_{gap} = 3.75$, the maximum stress is located in a small area just in the middle of the elementary cell; the stress gradient remains small in the loading direction, while it decreases quickly on the transverse axis. For higher distances from the pole, the analysis of the deformation fields reveals we can assume quasi-homogeneous stresses along the loading axis.

## Discussion

The main assumption of the model was the equal spacing between the spheres inside one chain. But also we have neglected interactions between chains of spheres. Some attempt in order to evaluate the importance of interchain interactions can be obtained from FEM simulations of cells containing for instance four particles disposed either on a square or in staggered position.

The results have shown that the chains do not interact each other. The reason is that the size of the region where the stress is concentrated inside: the gap between two spheres in is at least an order of magnitude smaller than the average distance between two chains. The strain map shows that the region separating the chains is almost not deformed, even if the chains are staggered, that is to say if the gap of one chain coincides with the equator of a particle on the adjacent chain; that is why the macroscopic stress does not differ from the single chain model.

The agreement between experiment, model and simulations is quite satisfying. This means that the structured composite can be described as a single chain structure. This simplification of the problem will facilitate the understanding of the magnetorheological behavior of the smart composite.

## Conclusion

This study on the elastic properties of an elastomer containing particles arranged in linear chains has shown firstly that this ordering strongly increases the elastic modulus compared to the case where the fillers are homogeneously distributed. On the other hand, the Mullins effect is very large giving rise to a final modulus, after a few tractions, which is close to the one of a composite with homogeneously distributed charge. Using a coupling agent strongly changes the slope of the first traction curve, giving a good indication of the effectiveness of the chemical grafting between particles and elastomeric network. A model based on lubrication type analysis well reproduces the elastic behavior of a two spheres experiment below the breaking strain. Thanks to this model we were able to show that, in the composite material, particles are not in contact inside the elastomer and that the average gap between particles was 5.6% of the radius. This finding is confirmed by electronic microscopy. Lastly a FEM analysis of the strain map has shown that the maximum stress is located on the surface of the particle at about 15° from the pole if the local strain is smaller than 40%, but that it moves to the center of the gap at higher strains. This last result is of interest relatively to debonding or tearing mechanisms involved at high local strains. It means that, if the coupling between particles and elastomer is weak, then debonding from the surface will start suddenly on a quite large area; on the contrary, for strong enough attachment, the elastomer will tear on the axis of centers and at the middle of the gap. These different modes of ruptures should give rise to different viscoelastic behavior depending on the grafting agent on the surface of the particles. This will be the object of a forthcoming paper.

## References

1. Occiuzzi A, Spizzuoco M, Serino G (2003) Smart Mater Struct 12:703
2. Dyke S, Spencer B, Sain M, Carlson J (1996) Smart Mater Struct 5:565
3. Yalcintas M, Dai H (1999) Smart Mater Struct 8:560
4. Genc S, Phule P (2002) Smart Mater Struct 11:140
5. Carlson J, Jolly M (2000) Mechatronics 10:555
6. Ginder J, Nichols M, Elie L, Tardiff J (1999) SPIE Conf Smart Mater Technol kll:131
7. Bellan C, Bossis G (2002) Int J Mod Phys B 16:2447
8. Jolly M, Carlson J, Munoz B, Bullions T (1996) J Intell Mater Syst Struct 7(6):613
9. Laraba-Abbes F, Ienny P, Piques R (2003) Polymer 44:821
10. Mullins L (1948) Rubber Chem Technol 46(1):281
11. Govindjee S, Simo J (1992) Int J Solids Struct 29(14/15):1737
12. Gent A, Park B (1984) J Mater Sci 19:1947
13. Vicente J, Bossis G, Lacis S, Guyot M (2002) J Magn Mat 251:100
14. Moshev V, Kozhevnikova L (1996) J Adhesion 55:209
15. Sadeghipour WWUK, Boberick K, Baran G (2002) Mat Sci Eng A, 332:362
16. Christensen R (1979) Mechanics of composite materials. Wiley. ISBN 0-89464-501-3